

Proton-Nucleus Elastic Scattering at 9.8 Mev*†

NORTON M. HINTZ

University of Minnesota, Minneapolis, Minnesota

(Received January 17, 1957)

The differential cross section for proton-nucleus elastic scattering has been measured for Li, N, Al, A, Ni, Cu, Ag, Sn, and Au at a laboratory proton energy of 9.8 Mev. Data were taken at 5° intervals from 15° to 170° with an estimated standard deviation of 3 to 5%. The 24-inch-diameter scattering chamber is described. The protons are detected by a NaI(Tl) crystal whose energy resolution was about 2.5% so that in almost all cases inelastic protons were rejected. The data for Al, A, Ni, Cu, Sn, and Au have been analyzed by using the optical model with the Saxon potential. Good fits are obtained for a radius constant $r_0 = 1.20$ in the formula $R = r_0 A^{1/3} \times 10^{-13}$ cm and a real well depth of 62 Mev for most elements. The imaginary well depth and the smoothing parameter are A -dependent. A brief discussion is given on the determination of nuclear radii from elastic scattering and nuclear reaction cross sections.

I. INTRODUCTION

THE detailed, systematic study of proton-nucleus elastic scattering began with the work of Cohen and Neidigh¹ at 22 Mev. They found diffraction-like patterns for fifteen elements from Be to Th, which they understood in terms of the diffraction of a plane wave by a sphere of radius proportional to $A^{1/3}$. Other proton-nucleus elastic scattering experiments have shown the same general features.²⁻¹⁵ The positions of the diffraction maxima and minima vary smoothly with A and with the proton energy, E . In a few cases the heights of the maxima or the depths of the minima are observed to change rapidly for relatively small changes in proton energy^{11,16,17} or in atomic number.¹⁴ It is not yet clear whether these variations are outside of what might be predicted by the optical model.

Neutron,¹⁸ alpha-particle,¹⁹⁻²³ and electron²⁴ elastic

scattering angular distributions also exist for a range of energies and nuclei.

This body of data, as it is being analyzed with the assumption of smooth charge and nuclear potential distributions, is yielding precise information on the radius, shape, and strength parameters of nuclei. The optical model is in some cases giving extremely good fits to the proton²⁵ and alpha²⁶ scattering experiments.

At the time the experiments reported here were begun, very few proton elastic data below 17 Mev existed. In addition, the first stage of the Minnesota proton linear accelerator had just come into operation, providing a highly collimated, monoenergetic beam of protons at 9.8 Mev. Thus, it seemed worthwhile to measure a number of elements at this energy. This is about the lowest energy at which the scattering would not be complicated by elastic contributions from the compound nucleus.

II. EXPERIMENTAL DETAILS

A. General

Fairly conventional elastic-scattering techniques were used, so the discussion will be brief.

Protons from the first section of the Minnesota three-stage Linac were magnetically deflected by about 30°, through holes in the second vacuum tank and rf cavity, and into the scattering area. These protons were focused by a three-element magnetic quadrupole lens into a 1/4-in. spot at the input collimating diaphragm.

The beam-collimating system (two 3/8-in. holes 30 in. apart) limited the angular divergence of the beam to $\pm 0.4^\circ$. Antiscattering apertures were provided. The

* A preliminary report of this work was presented at the 1955 winter meeting of the American Physical Society in Los Angeles [N. M. Hintz, Phys. Rev. **100**, 1794(A) (1955)].

† Supported in part by the U. S. Atomic Energy Commission.

¹ B. L. Cohen and R. V. Neidigh, Phys. Rev. **93**, 282 (1954).

² J. W. Burkig and B. T. Wright, Phys. Rev. **82**, 451 (1951).

³ Baker, Dodds, and Simmons, Phys. Rev. **85**, 1051 (1952).

⁴ P. C. Gugelot, Phys. Rev. **87**, 525 (1952).

⁵ L. M. Goldman, Phys. Rev. **89**, 349 (1953).

⁶ B. T. Wright, University of California Radiation Laboratory Report, UCRL-2422 (unpublished).

⁷ Burcham, Gibson, Hossain, and Rotblat, Phys. Rev. **92**, 1266 (1953).

⁸ G. Fischer, Phys. Rev. **96**, 704 (1954).

⁹ Freemantle, Prowse, and Rotblat, Phys. Rev. **96**, 1268 (1954).

¹⁰ Freemantle, Prowse, Hossain, and Rotblat, Phys. Rev. **96**, 1270 (1954).

¹¹ B. B. Kinsey, Phys. Rev. **99**, 332 (1955).

¹² I. E. Dayton and G. Schrank, Phys. Rev. **101**, 1358 (1956).

¹³ J. Leahy, University of California Radiation Laboratory Report, UCRL-3273 (unpublished).

¹⁴ D. A. Bromley and N. S. Wall, Phys. Rev. **102**, 1560 (1956).

¹⁵ B. B. Kinsey and T. Stone, Phys. Rev. **103**, 975 (1956).

¹⁶ R. Sherr (private communication).

¹⁷ G. W. Greenlees and Professor W. E. Burcham, Office of Naval Research European Scientific Notes, No. 10-10 (unpublished), and private communication.

¹⁸ See D. J. Hughes and R. S. Carter, *Neutron Cross Sections—Angular Distributions*, Brookhaven National Laboratory Report BNL-400 (unpublished) for a summary of the neutron angular distribution measurements.

¹⁹ G. W. Farwell and H. E. Wegner, Phys. Rev. **95**, 1212 (1954).

²⁰ Wegner, Eisberg, and Igo, Phys. Rev. **99**, 825 (1955).

²¹ E. Bleuler and D. J. Tendam, Phys. Rev. **99**, 1605 (1955).

²² R. Ellis and L. Schechter, Phys. Rev. **101**, 636 (1956).

²³ Igo, Wegner, and Eisberg, Phys. Rev. **101**, 1508 (1956).

²⁴ See R. Hofstadter, Revs. Modern Phys. **28**, 214 (1956) for a summary of the electron scattering results.

²⁵ Glassgold, Cheston, Stein, Schuldt, and Erickson, following paper [Phys. Rev. **106**, 1207 (1957)]. See this paper for a review of earlier optical model calculations.

²⁶ Cheston, Glassgold, Stein, Schuldt, and Erickson, Bull. Am. Phys. Soc. Ser. II, **1**, 339 (1956), and W. B. Cheston and A. E. Glassgold, Phys. Rev. **106**, 1215 (1957). See also G. Igo and R. M. Thaler, Phys. Rev. **106**, 126 (1957).

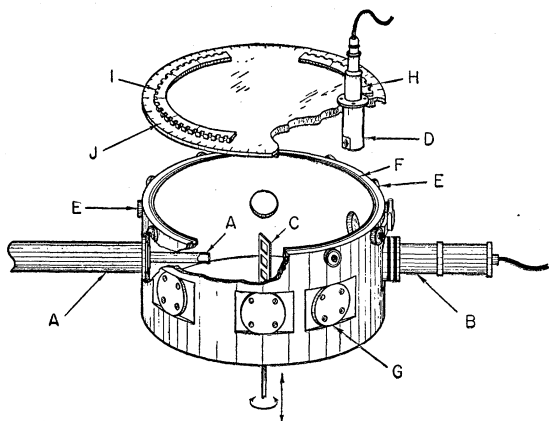


FIG. 1. Schematic drawing of 24 in.-diameter scattering chamber. *A*, input collimating and anti-scattering system; *B*, current collector; *C*, target frame; *D*, detector housing; *E*, roller bearings to support lid; *F*, O-ring groove; *G*, auxiliary ports; *H*, pre-amplifier; *I*, cog arrangement to advance lid; *J*, degree scale.

incident beam energy was 9.89 Mev with an energy spread of about 70 keV (full width at half-maximum). The maximum current that could be put into the chamber was about 10^{-8} ampere (time average) with a 1% duty cycle. For most runs, the current had to be reduced considerably below this value.

The scattering chamber, shown in Fig. 1, merits a brief description.²⁷ The chamber was constructed from a one-inch steel plate, rolled and welded to form a cylinder of 24-in. i.d. and 12-in. depth. O-ring grooves were cut in the top and bottom edges for sealing the covers. The bottom cover was bolted in place and contains an aperture at the center for either a solid target holder which could be externally positioned, or for gas lines leading to a small-volume, thin-walled, gas cell.²⁸ The top cover, which supports the detector, rests on twelve roller bearings which provide accurate positioning and which take the atmospheric load when the chamber is evacuated. The bearing height is adjusted to provide the minimum O-ring pressure necessary to provide a rotating vacuum seal. A degree scale is inscribed along the periphery of the lid. With a lever and cog arrangement, the lid can be adjusted in position to within $\pm 0.05^\circ$.

The detector,²⁹ which is at atmospheric pressure, is mounted in a re-entrant housing which hangs through a hole in the top cover of the chamber. It consists of a thin ($\sim \frac{1}{32}$ -in.) freshly cleaved NaI(Tl) crystal cemented to one face of a Lucite prism. The other face of the prism, at 90° to the crystal, was cemented to the window of a Dumont 6292 photomultiplier. This assembly is sealed into a brass housing, the inside of which is smoked with magnesium oxide. The scattered particles enter the

crystal through a Dural window $\frac{3}{8}$ in. in diameter and $\frac{1}{2}$ mil thick. The best resolution obtained with this arrangement was 2%, full width at half-maximum. This is shown in the pulse-height distribution of Fig. 2. In a period of several months the resolution would slowly deteriorate to about 3½%, after which a fresh crystal would be mounted.

For gas targets, a small volume cell,²⁸ $3\frac{3}{8}$ -in. diam by $1\frac{5}{8}$ in. high, of $\frac{1}{2}$ -mil Dural, was used, together with a detector collimating telescope which prevented the detector from seeing the intersection of the incident beam with the walls of the cell.

B. Operation and Treatment of Data

The detector pulses were amplified with conventional pulse equipment and presented to a 10-channel analyzer.

The straight-through beam was caught in a Faraday cup and integrated electronically, with an over-all uncertainty of about 1½%.

The Linac duty cycle is about 1% (200- μ sec pulse, 60 pulses per second) so pile up and dead time effects can be serious. Target thickness, detector geometry, and counting rates were chosen so that corrections to the data for dead-time and pile-up losses, multiple scattering in the target, and first- and second-order geometry factors were negligible at angles greater than 30° , and within the over-all uncertainty of the data at smaller angles.

A measurement of the left-right asymmetry of the scattered protons was made to determine the true zero of the degree scale. An error of 0.5° was found and the data were corrected accordingly.

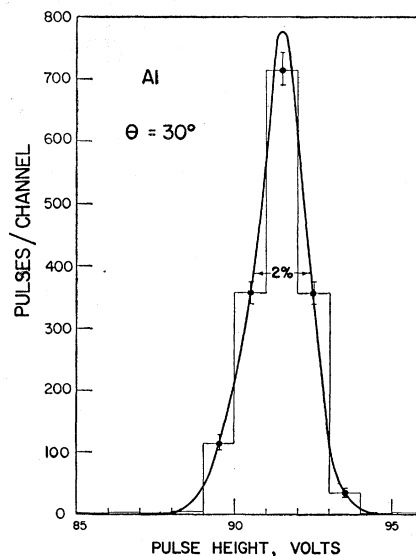


FIG. 2. Pulse-height distribution showing the best resolution obtained from a freshly cleaved crystal. Pulses from protons leaving Al in its first excited state would fall below 85 volts. The smooth curve is drawn by eye through the experimental histogram.

²⁷ The scattering chamber was designed by E. A. Day, N. M. Hintz, and L. H. Johnston.

²⁸ Allred, Rosen, Tallmadge, and Williams, *Rev. Sci. Instr.* **22**, 191 (1951).

²⁹ Ralph H. Lovberg, *Phys. Rev.* **103**, 1393 (1956).

For gas targets, a knowledge of the collected beam charge, gas pressure, and detector geometry enabled an absolute cross section to be calculated.

For the foil targets which were sufficiently uniform (Al, Ni), absolute cross sections were also calculated from beam current, target thickness, and detector geometry. In the remaining cases (Li, Cu, Ag, Sn, Au), the ratio of the observed cross section to Coulomb was arbitrarily normalized to be near unity at small angles. Since, for most elements, these ratios are still oscillating at the smallest angles for which data exist, the normalization must be considered as somewhat arbitrary.

The foils Au, Sn, Cu, Ni, and Al were of commercial origin. The Ag foil was prepared by electrodeposition. The Li foil (1 mil) was made by rolling Li metal with a glass roller under dry kerosene. The Li was then washed in *n*-decane and quickly put under vacuum. Scattering from any hydroxide layer on the Li could be resolved in the pulse-height analysis. The foil targets were about 200 kev thick, the gas targets about 50 kev. However, the energy loss in the Dural window of the gas cell reduced the proton energy at the center of the target to about the same value as for the foil targets. The average proton energy in the lab system for each target is given in Table I.

For the light elements (He³ through A⁴⁰), any inelastic proton groups could be almost completely resolved from the elastic in the pulse-height spectrum. In the worst cases (Li and Al), the maximum uncertainty in the elastic cross section due to unfolding the partially resolved inelastic peak was about $\pm 15\%$ for Li and $\pm 5\%$ for Al.

For Cu, Ni, Ag, and Sn, any appreciable excitation of the known levels would have been resolved except for the 0.09-Mev isomeric states of Ag. For Au, any excitation of the low-lying rotational states (of excitation $\lesssim 300$ kev) would be included under the "elastic" peak. However, from the shape of the pulse-height distribution it can be inferred that such excitation contributes not more than a few percent to the Au "elastic" cross section.

C. Results

The final results are shown in Figs. 3 through 5. All angles and cross sections have been transformed non-relativistically into the center-of-mass system. Counting statistics were generally $\pm 3\%$ (standard deviation) or

TABLE I. Average proton energy in the lab system, E_p , in Mev, for each element measured.

Element	E_p	Element	E_p
He ³	9.75	A	9.72
He ⁴	9.76	Ni	9.85
Li	9.80	Cu	9.75
Be	9.89	Sn	9.73
N	9.73	Ag	9.79
Al	9.85	Au	9.84

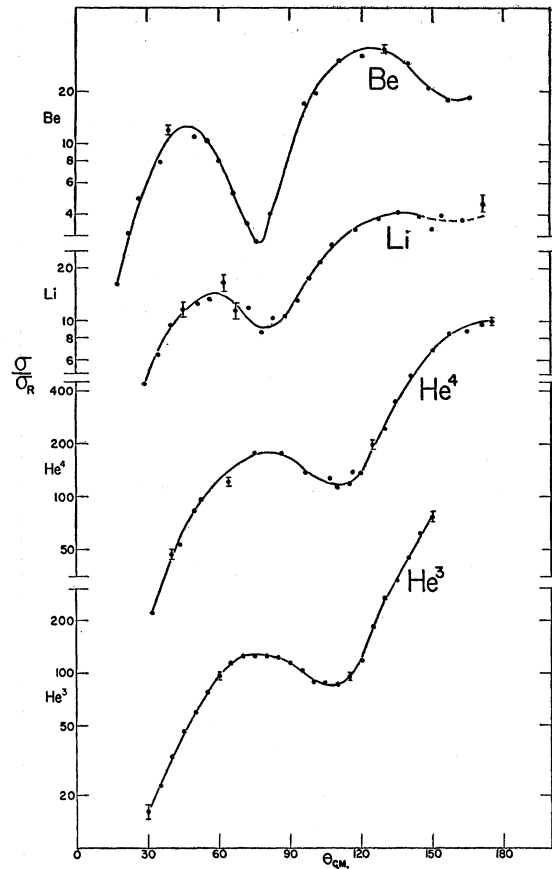


FIG. 3. Ratios of center-of-mass differential elastic scattering cross sections to Rutherford for He³ (reference 29), He⁴ (reference 30), Li, and Be (reference 31). The smooth curve was drawn by eye through the experimental points. Estimates of typical over-all errors are shown.

better. An estimate of the over-all errors in the final results due to statistics, current collection, and geometry factors is shown in the figures for typical points.

The data of several other workers at this laboratory have been included in the figures for the sake of completeness. The He³ data are by Ralph Lovberg,²⁹ the He⁴ by Williams and Rasmussen,³⁰ and the Be⁹ by Rasmussen.³¹ The Ni is a composite curve of unpublished data taken with the Los Alamos multiplate camera²⁸ by M. K. Brussel of this laboratory and of data taken by the author with the system described above.

The smooth variation with A in the position and relative strengths of the maxima and minima, even down to He³, can be seen in Figs. 3, 4, and 5.

The simple theory for the diffraction of a plane wave by a completely absorbing sphere of radius R leads to

³⁰ J. H. Williams and S. W. Rasmussen, Phys. Rev. **98**, 56 (1955).

³¹ Stanley W. Rasmussen, Phys. Rev. **103**, 186 (1956).

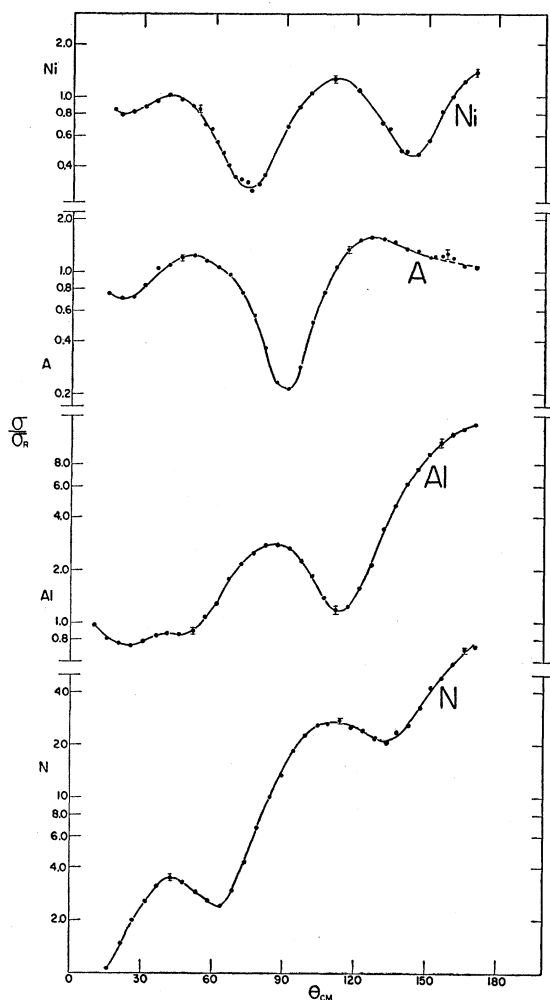


FIG. 4. Ratios of center-of-mass differential elastic scattering cross sections to Rutherford for N, Al, A, and Ni. The smooth curve was drawn by eye through the experimental points. Estimates of typical over-all errors are shown.

the expression³²

$$\sigma(\theta) \sim [J_1(kR \sin\theta)/\sin\theta]^2.$$

This expression is valid only for small angles. For a given feature of the diffraction pattern (e.g., a maximum or minimum) one would expect $kR \sin\theta$ to remain approximately constant as R is varied. There is no reason to expect such a simple picture to work in the case of diffraction by a partially transparent sphere when there are in addition complicated Coulomb-nuclear interference effects present. The best approximation to straight lines is in fact obtained if one plots $A^{-1/3}$ against simply θ , rather than $\sin\theta$. This is shown in Fig. 6. Except for the break in the curve for the first minimum and second maximum, the points lie reasonably well along straight lines. This apparently accidental scheme provides, at best, a useful interpolation device.

³² Fernbach, Serber, and Taylor, Phys. Rev. **75**, 1352 (1949).

III. CONCLUSIONS

It has been customary, lately, to discuss nucleon-nucleus elastic scattering in terms of the optical model.³³ The most extensive work to date on the analysis of proton elastic scattering has been done by Saxon and his collaborators³⁴ at the University of California at Los Angeles, and recently, by Glassgold *et al.*,²⁵ at the University of Minnesota. They have represented the proton-nucleus interaction by a complex central potential of the form:

$$V(r) = V_c(r) + Vf(r) + iWg(r), \quad (1)$$

where V_c is taken to be the Coulomb potential due to a uniform spherical (volume) charge of radius R ; V and W are constants; $f(r)$ and $g(r)$ are form factors. In the analysis of the data presented here, f and g were taken to be:

$$f(r) = g(r) = \left[1 + \exp\left(\frac{r-R}{a}\right) \right]^{-1}, \quad (2)$$

where $R = r_0 A^{1/3} \times 10^{-13}$ cm. A complete discussion of the work of Glassgold's group in fitting the 10-Mev data is

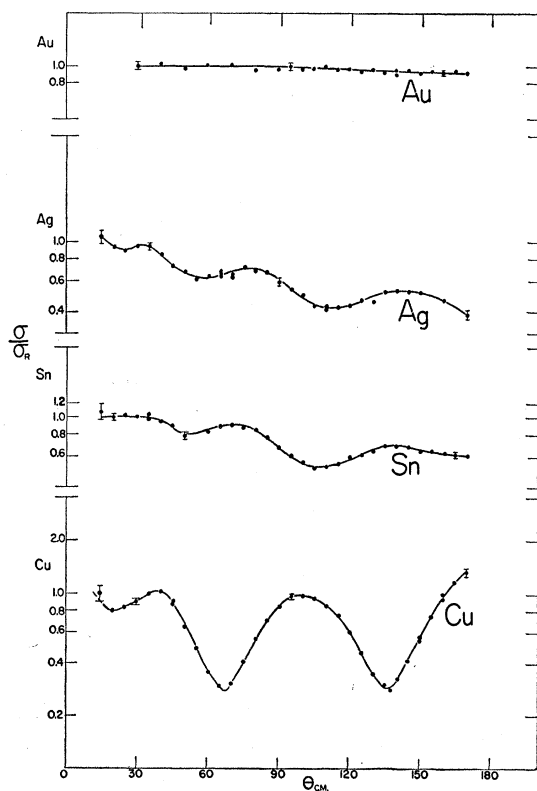


FIG. 5. Ratios of center-of-mass differential elastic scattering cross sections to Rutherford for Cu, Sn, Ag, and Au. The smooth curve was drawn by eye through the experimental points. Estimates of typical over-all errors are shown.

³³ H. A. Bethe, Phys. Rev. **57**, 1125 (1940).

³⁴ Melkanoff, Moszkowski, Nodvik, and Saxon, Phys. Rev. **101**, 507 (1956).

given in the following paper.²⁵ A few of their most important results will be summarized here.

The computations of Glassgold *et al.* consist of an exact numerical integration of the Schrödinger equation with the potential of Eqs. (1) and (2). A systematic procedure was devised which, after a few preliminary enlightened guesses as to the correct parameters, enabled them to converge on the best fit to the experimental points, as determined by a least-squares criterion. The best fits so obtained by using $r_0=1.20$ for A, Cu, and Sn are shown in Fig. 7. In the case of Au, no attempt was made to find the best fit since $\sigma/\sigma_R \sim 1$ over the entire angular range. A calculated curve for Au for a reasonable set of parameters is included in Fig. 7. This curve falls about 10% below Rutherford at back angles as is observed experimentally. Calculated curves for Al and Ni are given in the following paper. The parameters used in Fig. 7 are given in Table II. These fits are considerably better than any previously obtained with the optical model. This is partly due to the fact that no effort was made to find A -independent parameters giving the best average fit for a range of elements; each element was treated as a separate case.

The light elements, N through He³, have not been analyzed except for some preliminary unpublished work by Melkanoff and Saxon on N which, like Al, proves to be very difficult.²⁵

The most important conclusion of Glassgold's analysis is that, if one considers only the elastic scattering data, the parameters at 10 Mev are not unique. In cases where detailed explorations were made, equally good fits to the data could be obtained for a range of values of r_0 , providing V was adjusted to keep Vr_0^2 constant, and minor changes then made in a and W . This is discussed more thoroughly in the following paper. Except for the light elements, a good fit for all cases analyzed can be obtained for $r_0=1.20$. This is a somewhat smaller radius than has been previously found in the analysis of nuclear reaction and scattering experiments at energies <100 Mev.^{32,35} However, in those cases in which a large radius ($r_0 \sim 1.5$) is inferred from the experiments, the authors have used either the Fernbach, Serber, and Taylor³² (FST) semiclassical treatment of the optical model together with a square

TABLE II. Optical model parameters giving the best fit to experiment with $r_0=1.20$ for A, Cu, and Sn. The parameters used for Au, in Fig. 7, are also given although no attempt was made to discover the best-fit set. Energies are in Mev and lengths in 10^{-13} cm.

	r_0	a	V	W
A	1.20	0.41	-62	-9.5
Cu	1.20	0.52	-62	-8.6
Sn	1.20	0.54	-62	-6.9
Au	1.20	0.50	-62	-10

³⁵ See for example J. M. Blatt and V. F. Weisskopf, *Theoretical Nuclear Physics* (John Wiley and Sons, Inc., New York, 1952), p. 15.

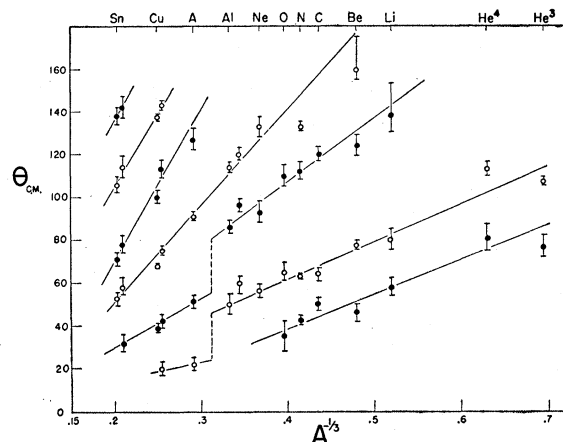


Fig. 6. Angles of successive maxima (black circles) and minima (open circles) in the ratio of elastic cross section to Rutherford vs $A^{-1/2}$. The straight lines were drawn by eye through the points.

well for the nuclear potential, or the compound-nucleus-formation cross sections tabulated in Blatt and Weisskopf³⁵ which have been calculated assuming a black, square well.

In the case of the optical model of FST, in its original form, the neglect of refraction by the potential (at least at energies $\lesssim 100$ Mev) and the use of a square rather than a smoothed well both tend to produce a large radius when theory is compared with experiment.

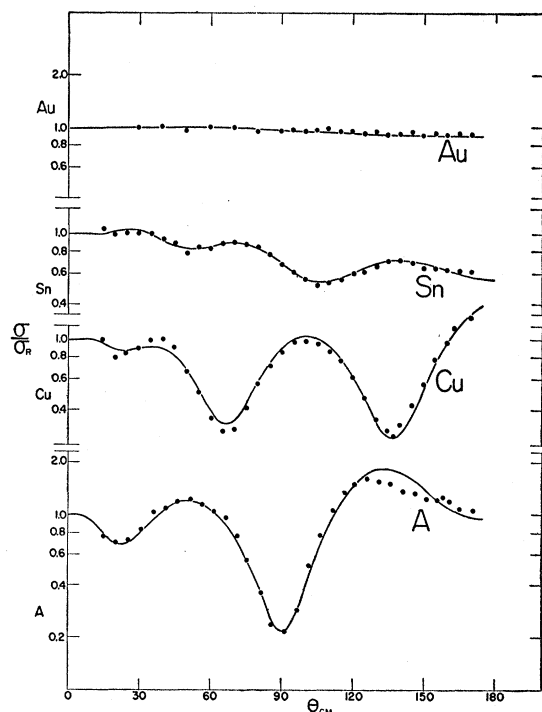


Fig. 7. Optical model fits to σ/σ_R for A, Cu, Sn, and Au. The values of the parameters used are given in Table II. The smooth curves are the optical model calculations, the circles the experimental points.

The reaction cross section at 10 Mev, calculated exactly with the Saxon potential, depends quite sensitively on a , the smoothing parameter. For example, a 10% increase in a (keeping R , V , and W fixed) produces about a 10% increase in σ_r for tin.³⁶ Thus, the tail of the Saxon potential gives a large contribution to the reaction cross section and it is to be expected that a square well, to produce the same cross section, would need to be of larger radius.

The black, square well approximation of Blatt and Weisskopf can also be expected to yield anomalously large radii when their values of σ_c , the cross section for compound nucleus formation, is compared with total reaction cross section data.³⁷ To take a particular example, if the total reaction cross section is calculated exactly, by using the optical model with the best-fit parameters for Cu and Sn, quoted in Table II, the values $\sigma_r = 664$ mb and 431 mb are obtained for Cu and Sn, respectively, at 9.75 Mev with a radius parameter, $r_0 = 1.20$. To obtain values this large from the black, square well approximation, a radius constant $r_0 = 1.5$ must be used. (The radius of the "equivalent" square well, having the same rms radius as a Saxon well with $r_0 = 1.20$ and $a = 0.5$, is $(r_0)_{s.w.} = 1.34$.)

In the few cases where rounded wells have been used, and the experiments are at sufficiently high energies that the FST optical model is expected to be a good approximation, a tapered well with the same rms radius as the Saxon potential with $r_0 \approx 1.2$ gives a good fit to the data.^{38,39} † Thus, in view of the work of Ross,

³⁶ A. E. Glassgold (private communications).

³⁷ See, for example, H. G. Blosser and T. H. Handley, *Phys. Rev.* **100**, 1340 (1955).

³⁸ Robert W. Williams, *Phys. Rev.* **98**, 1387 (1955).

³⁹ R. G. P. Voss and R. Wilson, *Proc. Roy. Soc. (London)* **A236**, 52 (1956).

† *Note added in proof.*—See however R. Wilson, *Phil. Mag.* **1**, 1013 (1956). The radius derived from an analysis of the small-angle neutron diffraction scattering at 136 Mev is inconsistent with the value, $r_0 = 1.20$ for a Saxon well, being approximately 15% higher.

Mark, and Lawson⁴⁰ which indicates that the *potential* radius is probably $\sim 1 \times 10^{-13}$ cm greater than the *charge* radius (for Au), it cannot at the present time be stated that the radius given by nuclear force experiments is inconsistent with that determined by electron scattering.

A remark should be made about the question of determining a unique set of optical model parameters since, as mentioned above, it appears that the 10-Mev elastic scattering data can be fitted by a range of values of r_0 , if suitable adjustments are made in the other parameters. These "equivalent" sets of optical model parameters predict slightly different total reaction cross sections at 17 Mev⁴¹ and at 10 Mev.²⁵ If r_0 is varied, always adjusting V , W , and a to give the best fit to the elastic angular distributions, the reaction cross sections predicted by the optical model seem to vary more rapidly at 10 Mev than at 17 Mev. This is probably because at 10 Mev the proton energy is near or below the Coulomb barrier energy and therefore the reaction cross section will depend very sensitively on the barrier height, and hence on r_0 . Accurate total reaction cross-section measurements at 10 Mev would be very helpful in settling the uniqueness question.

The purely geometric nuclear parameters, r_0 and a , can perhaps be determined more uniquely by analysis of elastic scattering experiments at higher energies. A program of elastic scattering at 40 Mev is now under way at this laboratory and will be reported in the near future.

ACKNOWLEDGMENTS

The author wishes to thank Professor L. H. Johnston, Dr. Ralph Lovberg, and Sheau-Wu Chen for assistance with various parts of the experiment. R. P. Featherstone and the members of the Linac crew were very helpful. Finally, the author is grateful to Professor J. H. Williams for his help and stimulation.

⁴⁰ Ross, Mark, and Lawson, *Phys. Rev.* **102**, 1613 (1956).

⁴¹ D. Saxon and M. A. Melkanoff (private communication).